European Journal of Drug Metabolism and Pharmacokinetics (2022) 47:855–868
https://doi.org/10.1007/s13318-022-00793-6

ORIGINAL RESEARCH ARTICLE

# Evaluating Islatravir Administered Via Microneedle Array Patch for Long-Acting HIV Pre-exposure Prophylaxis Using Physiologically Based Pharmacokinetic Modelling

**Hannah Kinvig[1] · Nicolas Cottura[1] · Andrew Lloyd[1] · Collrane Frivold[2] · Jessica Mistilis[2] · Courtney Jarrahian[2] · Marco Siccardi[1]**

Accepted: 2 August 2022 / Published online: 30 September 2022


## Abstract

**Background and Objectives** Technologies for long-acting administration of antiretrovirals (ARVs) for the prevention and treatment of HIV are at the forefront of research initiatives aiming to tackle issues surrounding drug adherence with the current standard of once-daily oral administration. Islatravir (ISL) is an emerging ARV that shows promising characteristics for long-acting prevention and treatment both orally as well as through alternative routes of administration. Microneedle array patches (MAPs) are a pain-free and discreet transdermal delivery technology that offer extended-release administration of nanoparticulate drugs. This study aimed to utilise physiologically based pharmacokinetic (PBPK) modelling to predict the pharmacokinetics resulting from ISL administered via MAP and to identify key MAP characteristics required to sustain effective concentrations over extended dosing intervals.

**Methods** A PBPK model describing the conversion of ISL to ISL-triphosphate (ISL-TP) and its whole-body disposition was developed and verified against observed clinical data for orally administered ISL in healthy adults. An intradermal PBPK model was integrated with the ISL PBPK model to predict the dose and nanoparticle release rate required for MAP administration strategies capable of achieving a minimum ISL-TP target concentration of 0.05 pmol/$10^6$ PBMCs over extended dosing intervals. MAP design was limited to a maximum therapeutic area of 20 $cm^2$ with a dose loading of 4.09 mg/$cm^2$ and a minimum duration of 3 months. Due to the lack of available clinical data, a range of nanoparticle release rates and MAP bioavailability scenarios were simulated to provide an overview of potential clinical outcomes.

**Results** The ISL PBPK model was successfully verified, with predicted vs observed ratios falling within 0.5–2-fold. ISL MAP doses ranging from 15 to 80 mg were predicted to sustain ISL-TP concentrations above the minimum target concentration at 3, 6 and 12 months after administration. Nanoparticle release rate and MAP bioavailability were found to have a major impact on whether dosing strategies achieved the criteria. Minimum doses of 15 mg and 60 mg with a nanoparticle release rate of 0.0005 $h^{-1}$ and bioavailability ranging from 25 to 100% were predicted to achieve effective ISL-TP concentrations up to 3 and 6 months, respectively. Doses of 15 mg and 30 mg with a nanoparticle release rate of 0.0005 $h^{-1}$ were also able to attain the target concentration up to 6 months after MAP administration, albeit with a minimum bioavailability of 75% and 50%, respectively. Furthermore, when simulating a bioavailability of 100%, an 80 mg ISL MAP was predicted to sustain ISL-TP concentrations above the minimum target concentration up to 12 months after administration.

**Conclusions** The ISL PBPK model successfully predicted ISL and ISL-TP pharmacokinetics across a range of orally administered regimens. The integrated intradermal PBPK model outlined optimal MAP dose and nanoparticle release rates for effective ISL-TP concentrations up to 12 months, providing justification for further investigation of ISL as a candidate for MAP administration.

Extended author information available on the last page of the article

**Key Points**

The physiologically based pharmacokinetic model in this study predicted that the transdermal delivery of islatravir through microneedle array patches $\leq 20\ cm^2$ was able to achieve plasma concentrations above the minimum target 3, 6 and 12 months after administration with doses ranging from 15 mg to 80 mg.

Our study provides rationale for the further investigation of islatravir as a candidate for microneedle array patch administration.

## 1 Introduction

In 2020, there were approximately 37.7 million people living with HIV (PLWH) globally, with an estimated 74% receiving antiretroviral therapy (ART) [1]. ART currently consists of two- or three-drug regimens containing orally administered antiretrovirals (ARVs). ARVs can also be utilised for pre-exposure prophylaxis (PrEP) and post-exposure prophylaxis (PEP) in HIV-negative individuals encountering high-risk HIV exposures [2, 3]. ARVs target the HIV life cycle process both before and after HIV infiltration of the host cell, whilst some ARVs act as pharmacokinetic enhancers to enable effective therapeutic plasma concentrations [4–6]. Several ARVs are currently available for prevention and treatment. New ARVs are also in development to attain high potency while minimising the toxicity and drug interaction profile [7]. Moreover, long-acting ARVs are of increasing interest, with the notion being to reduce pill burden and issues surrounding drug adherence which are currently barriers to ART uptake and effectiveness [8, 9]. Additionally, several patient surveys have found high rates of interest in long-acting alternatives for HIV treatment and prevention [9]. To address these gaps in ART delivery and adherence, Cabenuva, which is a combination of cabotegravir (CAB) and rilpivirine (RPV) administered intramuscularly (IM), was approved by the FDA for the treatment of HIV in January 2021. Cabenuva is effective for once-monthly administration with studies indicating potential for administration every 2 months [10, 11]. However, alternative administration strategies remain of interest due to the disadvantages of IM formulations, including the need for administration by a skilled health worker, logistical challenges surrounding frequent clinic visits and resulting stigma [8, 9].

Microneedle array patches (MAPs) are a pain-free and discreet administration technique that consist of micron-scale needles capable of long-acting transdermal nanoparticulate drug delivery. MAP technologies have received increasing research efforts in the recent past, with their application extending beyond ART [12]. MAPs could help overcome the adherence issues surrounding oral administration whilst providing a potentially favourable administration route to IM injection for long-acting prevention and treatment of HIV. Drugs suitable for MAP delivery are characterised as highly potent with a long half-life, resulting in low doses capable of sustaining effective plasma concentrations over extended periods of time whilst maintaining appropriate MAP sizes [9, 13–16]. Islatravir (ISL) is a highly potent nucleoside reverse transcriptase translocation inhibitor with a long half-life that is currently being evaluated across multiple clinical trials for the prevention and treatment of HIV [17–22]. ISL prevents HIV replication through several unique mechanisms that are distinct from other nucleoside reverse transcriptase inhibitors [20, 23]. ISL enters peripheral blood mononuclear cells (PBMCs) where it undergoes rapid conversion via endogenous intracellular kinases to its active form, ISL-triphosphate (ISL-TP), before slowly converting back to ISL and re-entering the systemic circulation [24]. ISL has demonstrated a favourable long-acting profile, highlighting its potential for an extended duration of protection through MAP delivery [17, 20, 25].

Physiologically based pharmacokinetic (PBPK) modelling is an in silico technique that uses mathematical equations to describe the ADME processes and physiological characteristics of the human body as well as various species such as rats. Virtual cohorts of patients can be simulated for the prediction of drug pharmacokinetics resulting from numerous routes of administration and regimens by incorporating drug-specific physicochemical properties [26]. PBPK modelling can be employed for the investigation of ISL MAPs for ART by predicting clinical outcomes and highlighting MAP design requirements. A MAP intradermal PBPK model was previously reported and describes the movement of the drug through the stratum corneum, viable epidermis, and dermis whilst considering specific MAP characteristics [27]. The model was adapted and modified from a dermal PBPK modelling study that found that by considering skin sub-compartments and hair follicles, more accurate predictions could be made versus models with simpler structures [28]. The MAP intradermal PBPK model was successfully developed utilising rat *in vivo* data for nanoparticulate CAB and RPV and was applied for the prediction of CAB and RPV MAPs in humans [27].

The aim of this study was to develop and verify a whole-body PBPK model describing the conversion of ISL to ISL-TP for the prediction of ISL MAP pharmacokinetics. The study aimed to provide preliminary data to identify optimal dosing strategies, nanoparticle release rates and resulting MAP characteristics capable of sustaining effective ISL-TP concentrations to aid in future ISL MAP research initiatives.

## 2 Methods

A PBPK model was developed for ISL in Simbiology v5.8, a product of Matlab 2018a (MathWorks, Natick, MA, USA). Drug distribution in the intradermal MAP compartments was described using permeability-limited, first-order kinetics. The drug distribution in the remaining whole-body PBPK model was described using blood-flow-limited, first-order kinetics with well-stirred compartments that assumed instant distribution of the drug. Furthermore, it was assumed that there was no absorption of orally dosed drug from the large intestine. Physicochemical, pharmacokinetic, *in vitro*, and *in vivo* data for ISL and ISL-TP were sourced from the literature or, if unavailable, were estimated via curve fitting to the observed clinical data. Where applicable, concentration–time profile data were extracted from graphs using the Plot Digitizer Tool v4.5 (WebPlotDigitizer, Pacifica, California, USA). The PBPK model was verified against observed clinical data for both ISL and ISL-TP. Specifically, clinical data for ISL 0.5–30 mg single oral dose and ISL 60 mg and 120 mg once-monthly oral dose regimens were used. For model verification and application, virtual cohorts consisting of 50 male and 50 female patients aged 18–60 years were simulated.

### 2.1 Whole-Body PBPK Model

Weight and body mass index for virtual male and female patients aged 18–60 years were defined using data from the National Center for Health Statistics [29] and used to determine height and body surface area [30, 31]. These characteristics were applied in anthropometry equations to calculate organ weight [30], with organ density being implemented alongside weight to determine organ volume [32]. Furthermore, blood flow rates were defined as a fraction of the total cardiac output [33]. A multi-compartment absorption and transit model was implemented for the simulation of oral absorption [26, 34, 35]. Volume of distribution was calculated as previously described, with the zwitterionic olive oil:buffer partition coefficient ($\log D^{*}_{\mathrm{vo:w}}$) equation being applied for ISL [36]. The systemic circulation of ISL was calculated through previously reported differential equations for eliminating and non-eliminating organs [34]. A schematic representation of the whole-body PBPK model, including the MAP and PBMC compartments, can be found in Fig. 1 [37]. The physicochemical and pharmacokinetic input parameters for the simulation of ISL in the PBPK model are shown in Table 1. To note: the blood-to-plasma ratio ($R$) of ISL was calculated using Eqs. 1–4 in the Supplementary Material due to a lack of available data [38].

The conversion pathway of ISL to ISL-TP [24] was integrated into the whole-body PBPK model using Eqs. 1–3, with a schematic representation being shown in Fig. 2. $A_{\mathrm{vein,ISL}}$, $A_{\mathrm{PBMC,ISL,in}}$ and $A_{\mathrm{PBMC,ISL,out}}$ are the amounts of ISL in the vein compartment, entering the PBMC compartment, and leaving the PBMC compartment, respectively. $A_{\mathrm{PBMC,ISLTP}}$ is the amount of ISL-TP in the PBMC compartment. $K_{\mathrm{in,ISL}}$ and $K_{\mathrm{out,ISL}}$ are the rates at which ISL enters and leaves the PBMC compartment, respectively. $K_{\mathrm{ISL,ISLTP}}$ and $K_{\mathrm{ISLTP,ISL}}$ are the rates of ISL conversion to ISL-TP and ISL-TP conversion to ISL, respectively. Due to a lack of data, $K_{\mathrm{in,ISL}}$, $K_{\mathrm{out,ISL}}$, $K_{\mathrm{ISL,ISLTP}}$ and $K_{\mathrm{ISLTP,ISL}}$ were estimated via curve fitting. This process was carried out in a stepwise manner whereby initial values for each parameter were selected based on the rapid conversion of ISL to ISL-TP and slow return of ISL-TP to ISL within PBMCs, as outlined in the literature [24]. Each value was optimised incrementally until the ratio of predicted vs observed and the absolute average fold error (AAFE) values for the 0.5–30 mg oral regimens fell within the verification criteria [17]. The optimised values underwent secondary verification through the simulation of the 60 mg and 120 mg oral once-monthly ISL regimens [22]. Additionally, $1.17 \times 10^{9}$ PBMCs per litre of blood were considered in the PBPK model [44].

$$\frac{\mathrm{d}A_{\mathrm{PBMC,ISL,in}}}{\mathrm{d}t} = K_{\mathrm{in,ISL}} \times A_{\mathrm{vein,ISL}} - K_{\mathrm{ISL,ISLTP}} \times A_{\mathrm{PBMC,ISL,in}} \quad (1)$$

$$\frac{\mathrm{d}A_{\mathrm{PBMC,ISLTP}}}{\mathrm{d}t} = K_{\mathrm{ISL,ISLTP}} \times A_{\mathrm{PBMC,ISL,in}} - K_{\mathrm{ISLTP,ISL}} \times A_{\mathrm{PBMC,ISLTP}} \quad (2)$$

$$\frac{\mathrm{d}A_{\mathrm{PBMC,ISL,out}}}{\mathrm{d}t} = K_{\mathrm{ISLTP,ISL}} \times A_{\mathrm{PBMC,ISLTP}} - K_{\mathrm{out,ISL}} \times A_{\mathrm{PBMC,ISL,out}}. \quad (3)$$

### 2.2 MAP Intradermal PBPK Model

The MAP intradermal PBPK model was previously described, with a schematic representation being shown in Fig. 3 [27]. Due to limited data, the MAP formulation dose loading of 4.09 mg/cm$^2$ applied for CAB and RPV was also used for ISL. The partition coefficient and permeability coefficient input parameters describing the movement of ISL throughout the skin layers were calculated using the average value from collated quantitative structure–property relationship (QSPR) equations [27, 28]. The partition coefficient and permeability coefficient input parameters for ISL are shown in Table 2. Similarly to the previously described MAP intradermal PBPK model, the rate of transfer of free drug between skin layers was assumed to be 1 h$^{-1}$ [27].

### 2.3 PBPK Model Verification

The reported MAP intradermal PBPK model utilised in this study was previously verified. Briefly, the PBPK model was successfully verified against CAB and RPV rat and human

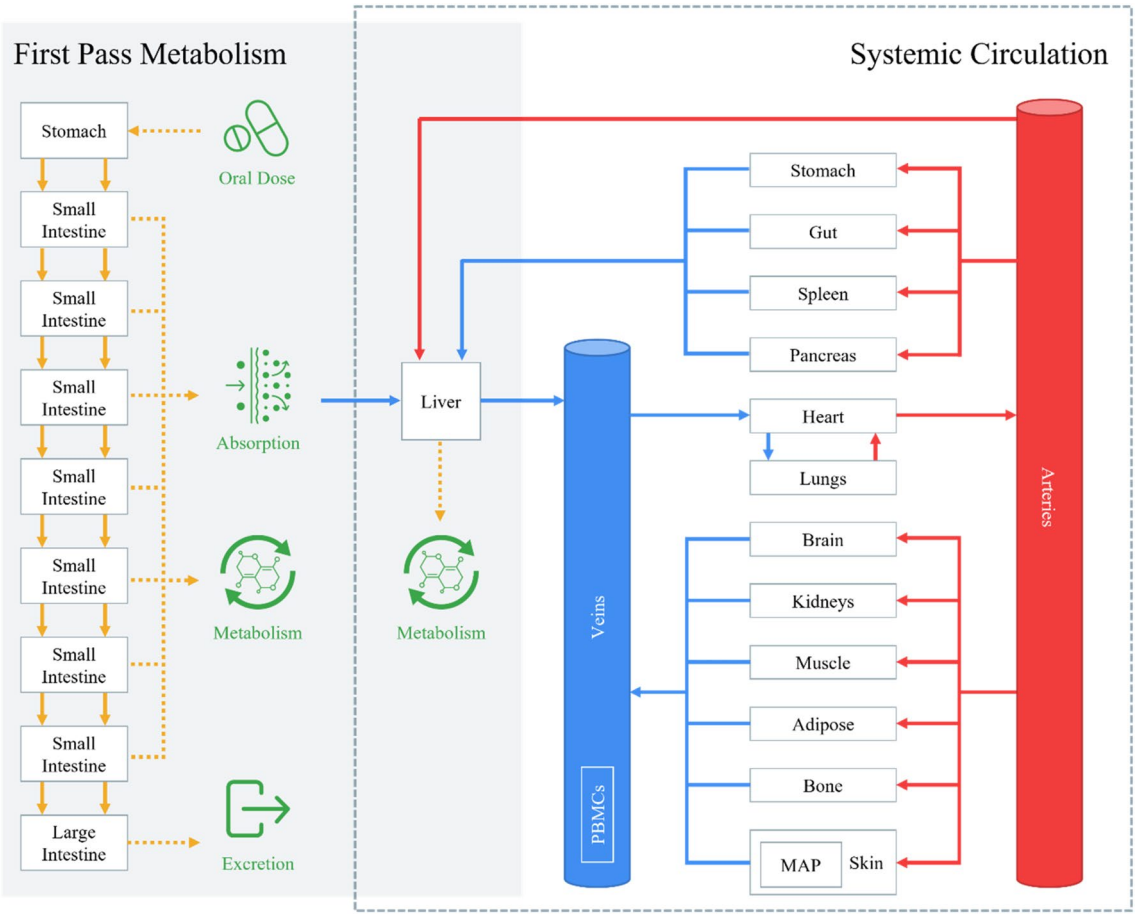


**Fig. 1** Schematic diagram of the whole-body PBPK model used to predict ISL and ISL-TP pharmacokinetics after oral administration. Organs, tissues, PBMCs and the MAP are represented by *compartments*, with the drug distribution represented by *arrowed lines*. Veins, arteries and their associated reactions are highlighted in *blue* and *red*, respectively, with reactions involved in absorption, metabolism and excretion highlighted in *yellow*. Compartments and reactions involved in first-pass metabolism are located within the *grey box*, with those involved in systemic circulation enclosed within the *dashed line*. *PBPK* physiologically based pharmacokinetic modelling, *ISL* islatravir, *ISL-TP* islatravir triphosphate, *PBMCs* peripheral blood mononuclear cells, *MAP* microneedle array patch

intramuscular injection pharmacokinetic data alongside intradermal MAP pharmacokinetic data in rats [27]. Moreover, the whole-body PBPK model with the integrated ISL to ISL-TP conversion mechanism developed herein was considered successfully verified if the ratio of predicted vs observed pharmacokinetic values for orally administered ISL and ISL-TP was between 0.5-fold and 2-fold [45]. In addition, the absolute average fold error (AAFE) for the predicted vs observed pharmacokinetic parameters and concentration–time profiles were also calculated, as defined in Eq. 4, where $N$ is the number of data points [46]. AAFE values between 1 and 2 were considered successfully verified.

$$\mathrm{AAFE} = 10^{\left|\frac{1}{N}\Sigma\log\frac{\mathrm{Predicted}}{\mathrm{Observed}}\right|} \quad (4)$$

## 2.4 Prediction of Islatravir MAP Pharmacokinetics

Dosing strategies for ISL MAP simulations were based upon a maximum therapeutic area of 20 $cm^2$ (assuming a dose loading of 4.09 $mg/cm^2$ [27]), a minimum ISL-TP target concentration of 0.05 $pmol/10^6$ PBMCs [22] and a minimum duration of 3 months. Simulations aimed to determine the maximum dosing interval achievable under these criteria. To provide an overview of potential clinical scenarios, nanoparticle release rates of 0.005 $h^{-1}$, 0.0025 $h^{-1}$ and 0.0005 $h^{-1}$ were simulated based upon the previously reported MAP intradermal PBPK model study [27]. Additionally, due to the lack of data, a range of bioavailability scenarios which account for MAP delivery efficiency and movement of ISL from the skin into systemic circulation from 25 to 100% were simulated for each MAP dose.

**Table 1** Physicochemical and pharmacokinetic input parameters for the ISL PBPK model

| Parameter | ISL | Reference |
|---|---|---|
| Molecular weight (g/mol) | 293.5 | [39] |
| HBD | 3 | [39] |
| log$P_{O:W}$ | 0.55 | [40] |
| $P_{app}$ (cm/s) | $6.265 \times 10^{-7}$ | [41] |
| p$K_a$ | 13.32, 0.79 | [42] |
| Protein binding (%) | 98 | [43] |
| PSA (Å$^2$) | 119 | [39] |
| *R* | 1[a] | [38] |
| Water solubility (mg/L) | 744 | [42] |
| Bioavailability | 1 | [42] |
| Apparent clearance (L/h) | 31 | [17] |

*ISL* islatravir, *HBD* hydrogen bond donor, *log* $P_{O:W}$ partition coefficient between octanol and water, $P_{app}$ apparent permeability, $pK_a$ logarithmic value of the dissociation constant, *PSA* polar surface area, *R* blood-to-plasma ratio

[a]Calculated using equations provided in the reference

## 3 Results

### 3.1 PBPK Model Verification

The PBPK model was successfully verified according to the criteria by comparing the predicted area under the curve (AUC), maximum concentration ($C_{max}$), concentration at 168 h ($C_{168}$), and concentration–time profiles with the observed clinical data for the oral administration of ISL and its product ISL-TP. The AAFE and ratio verification results for the predicted ISL and ISL-TP pharmacokinetics from single-dose oral ISL regimens can be found in Tables 3 and 4, respectively [17]. The predicted concentration–time profiles of ISL-TP resulting from single-dose oral ISL regimens can be found in Figs. 1–5 of the Supplementary Material. The predicted concentration time profiles of ISL-TP resulting from once-monthly 60 mg and 120 mg oral doses of ISL can be found in Figs. 4 and 5, respectively [22]. The parameters applied in the model to describe the conversion of ISL to ISL-TP were estimated via curve fitting to the observed clinical data.

Parameters $K_{in,ISL}$, $K_{ISL,ISLTP}$, $K_{ISLTP,ISL}$ and $K_{out,ISL}$ were estimated as 4 h$^{-1}$, 4 h$^{-1}$, 0.006 h$^{-1}$ and 1 h$^{-1}$, respectively, via curve fitting to the available clinical data. Furthermore, the equation calculating $K_a$ [34] was unable to accurately describe the absorption of oral ISL, and so this value was also estimated via curve fitting to equal 1.5 h$^{-1}$.

### 3.2 Predicted ISL MAP Pharmacokinetics

The MAP intradermal PBPK model was integrated into the verified ISL PBPK model for the simulation of ISL MAPs. Release rates of 0.005 h$^{-1}$, 0.0025 h$^{-1}$ and 0.0005 h$^{-1}$ were considered alongside ISL MAP bioavailability ranging from 25 to 100% to provide an overview of potential clinical scenarios. A maximum therapeutic area of 20 cm$^2$ (4.09 mg/cm$^2$ dose loading) and a minimum ISL-TP concentration of 0.05 pmol/10$^6$ PBMCs was targeted during MAP dosing simulations. The predicted ISL-TP $C_{min}$ at 3, 6 and 12 months after the administration of 15 mg (3.67 cm$^2$), 30 mg (7.34 cm$^2$), 60 mg (14.68 cm$^2$) and 80 mg (19.57 cm$^2$) ISL MAPs can be found in Tables 5, 6, 7 and 8, respectively.

All ISL MAP dosing regimens simulated across all bioavailability percentages with a release rate of 0.0005 h$^{-1}$ achieved the minimum target concentration 3 months after administration. MAP dosing of 30 mg, 60 mg, and 80 mg sustained concentrations above the minimum target at 3 months with a release rate of 0.0025 h$^{-1}$, although only the 80 mg dose was able to achieve this across all bioavailability scenarios. Similarly, all ISL MAP dosing regimens were able to achieve the minimum target concentration 6 months after administration with a release rate of 0.0005 h$^{-1}$. However, 15 mg and 30 mg MAP dosing were only able to attain this with select bioavailability rates (15 mg: 75%, 100%; 30 mg: 50%, 75%, 100%). Dosing regimens with a release rate of 0.0025 h$^{-1}$ did not achieve the minimum target concentration across any bioavailability scenario 6 and 12 months after administration. The simulated 80 mg ISL MAP sustained ISL-TP concentrations above the minimum target concentration up to 12 months after administration with a release rate of 0.0005 h$^{-1}$ and a bioavailability of 100%. MAPs with a release rate of 0.005 h$^{-1}$ did not achieve the minimum target concentration of ISL-TP for any dosing regimen at 3, 6 or 12 months after administration. Additionally, the time taken to reach the minimum target concentration after MAP administration increased with slower release rates, lower doses, and lower bioavailability. A maximum time of approximately 5 days was predicted to reach the minimum target concentration for the 15 mg ISL MAP with a bioavailability of 25% and release rate of 0.0005 h$^{-1}$.

## 4 Discussion

ISL is a potent ARV with promising characteristics for long-acting technologies [20]. Specifically, nanoparticulate ISL MAPs have the potential to provide pain-free and discreet long-acting administration for the prevention and treatment of HIV. In this study, the conversion of ISL to its active form, ISL-TP, was mathematically described and implemented in a MAP intradermal PBPK model [27]. Cohorts of virtual patients were simulated to predict optimal MAP dosing strategies and nanoparticle release rates to sustain effective ISL-TP concentrations over extended periods of time.

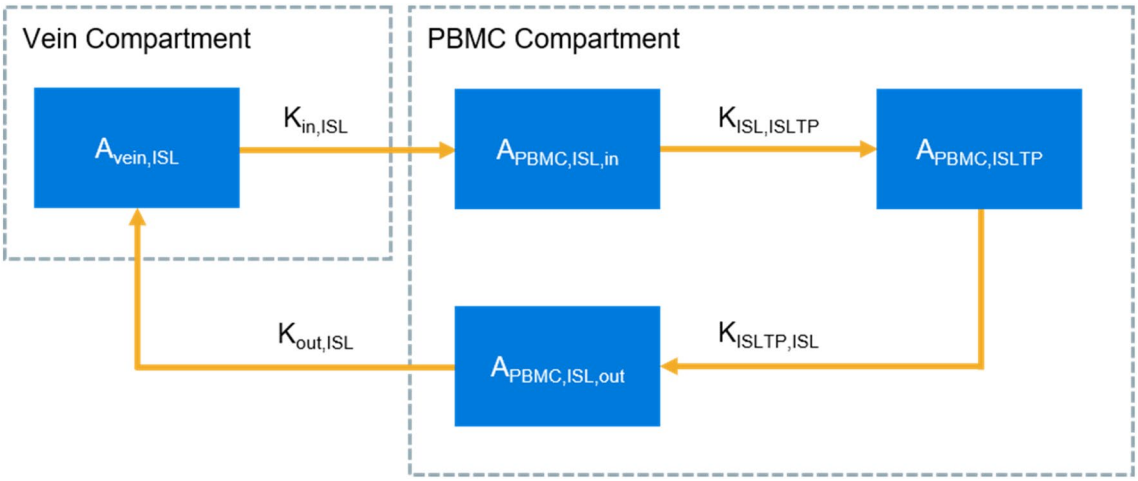


**Fig. 2** PBMC compartment structure describing the conversion pathway of ISL to ISL-TP integrated with the vein compartment of the whole-body PBPK model. *PBMC* peripheral blood mononuclear cells. $A_{vein,ISL}$, $A_{PBMC,ISL,in}$, $A_{PBMC,ISL,out}$ amounts of ISL in the vein compartment, entering the PBMC compartment and leaving the PBMC compartment, respectively; $A_{PBMC,ISLTP}$ amount of ISL-TP in the PBMC compartment; $K_{in,ISL}$, $K_{out,ISL}$ rates at which ISL enters and leaves the PBMC compartment, respectively; $K_{ISL,ISLTP}$, $K_{ISLTP,ISL}$ rates of ISL conversion to ISL-TP and ISL-TP conversion to ISL, respectively

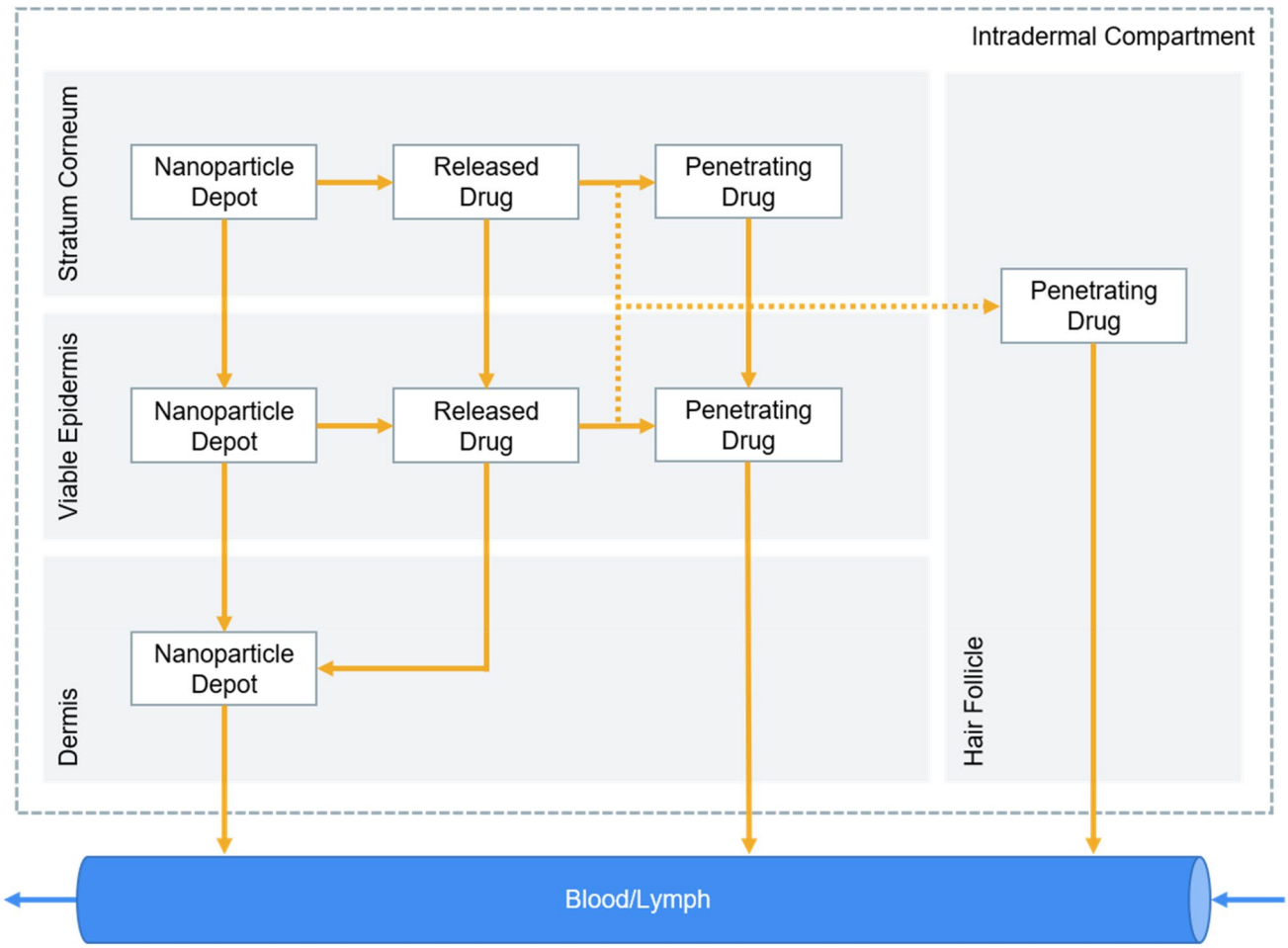


**Fig. 3** Schematic representation of the drug release pathway implemented in the MAP intradermal PBPK model. Diagram adapted from Rajoli et al. [27]

**Table 2** Calculated partition coefficient and permeability coefficient input parameters for the ISL MAP intradermal PBPK model [27]

| Parameter | ISL |
|---|---|
| $PC_{s/w}$ | $8.56 \times 10^{-3}$ |
| $PC_{sc/w}$ | 0.261 |
| $PC_{ve/w}$ | 0.124 |
| $PC_{w/sc}$ | 3.79 |
| $PC_{sc/ve}$ | 3.2 |

Partition and permeability coefficients calculated using QSPR equations as described previously [27]

*ISL* islatravir, $PC_{s/w}$ permeability coefficient between skin and water, $PC_{sc/w}$ permeability coefficient between the stratum corneum and water, $PC_{ve/w}$ permeability coefficient between the viable epidermis and water, $PC_{w/sc}$ partition coefficient between the stratum corneum and water, $PC_{sc/ve}$ partition coefficient between the stratum corneum and viable epidermis

The PBPK model describing the conversion of ISL to ISL-TP was successfully verified against multiple data sets for the oral single-dose ISL administration. There was a general trend for the PBPK model to underpredict the ISL-TP pharmacokinetics for 0.5 mg and 1 mg doses and overpredict the ISL-TP pharmacokinetics for 2 mg, 10 mg and 30 mg doses, as shown in Tables 3 and 4 and Figs. 1–5 in the Supplementary Material. These trends, alongside the available clinical data, suggest that the pharmacokinetics of ISL-TP are not necessarily dose proportional, contrary to what was previously reported [17]. However, the small patient sample size ($n = 6$) for the available oral single-dose ISL clinical data must be taken into consideration when analysing the verification data [17]. A larger sample size would be required to definitively assess whether ISL-TP pharmacokinetics are dose proportional before PBPK modelling strategies to describe non-linear drug pharmacokinetics could be justifiably implemented. Furthermore, due to the recent development of ISL, clinical pharmacokinetic data are scarce, and future PBPK modelling initiatives utilising emerging ISL clinical data will be essential for refining prediction accuracy. For example, the available apparent permeability data for ISL [41] was unable to accurately predict ISL absorption using the equation for $K_a$ in the model [34]. A previous study found that drugs with an effective permeability of lower than $1 \times 10^{-4}$ cm/s (ISL $P_{app} = 6.265 \times 10^{-7}$ cm/s) showed a wide range of fraction absorbed values, leading to techniques such as Caco-2 cell permeability proving unreliable in some instances. Under these circumstances, it is justifiable to utilise alternative means to calculate the fraction absorbed, hence the estimation of $K_a$ in this study in the absence of alternative $P_{app}$ data. In addition to the single-dose ISL clinical data, the PBPK model was successfully verified against clinical data for 60 mg and 120 mg once-monthly oral ISL administration [22]. Although these data sets were limited to the concentration–time profile alone, their likeness to the extended dosing intervals simulated for the ISL MAP regimens aids in model reliability.

The employed mechanism and estimated parameters describing the conversion of ISL to ISL-TP proved successful in simulating the ISL and ISL-TP pharmacokinetics. The mechanism was based on the uptake of ISL into PBMCs ($K_{in,ISL}$), where it then underwent rapid conversion via endogenous intracellular kinases to ISL-TP ($K_{ISL,ISLTP}$), before slowly converting back to ISL ($K_{ISLTP,ISL}$), followed by efflux out of the PBMCs ($K_{out,ISL}$) [24]. However, due to a lack of data, the parameters applied to describe this process were estimated and present a limitation of the current model, especially considering the limited availability of clinical data available for model verification. This current limitation could be resolved through the generation of *in vitro* and *in vivo* data describing the outlined parameters. Specifically, the concentration of ISL within PBMCs would provide us with additional confidence in parameter estimation, although this may be challenging to determine *in vitro* due to its rapid conversion to ISL-TP.

The ISL whole-body PBPK model integrated with the MAP intradermal PBPK model was used to predict the ISL and ISL-TP pharmacokinetics resulting from varying MAP design strategies to determine the long-acting administration potential of ISL. With the maximum therapeutic area of 20 $cm^2$ and dose loading of 4.09 $mg/cm^2$ [27] being the major limiting factors for MAP design in this study, the PBPK model predicted that doses of between 15 and 80 mg could sustain ISL-TP concentrations above the minimum target concentration over 3–12 months. Nanoparticle release rate and MAP bioavailability had a significant impact on the administration timeframe, whereby faster nanoparticle release rates and a lower bioavailability decreased the period of time that ISL-TP concentrations were greater than 0.05 $pmol/10^6$ PBMCs. As these two aspects of ISL MAPs are currently unknown, several scenarios were simulated to obtain a wider understanding of potential clinical outcomes and outline target characteristics for future MAP designs capable of long-acting administration; however, questions surrounding the practicality of these characteristics for ISL MAPs remain unanswered. Unlike the previously reported MAP intradermal PBPK model for CAB and RPV [27], the model applied herein was not verified against *in vivo* ISL MAP data due to its lack of availability, and this presents as a limitation of this study. Future *in vitro* and *in vivo* studies could fill the knowledge gap for various ISL MAP intradermal PBPK modelling, enabling more reliable predictions of clinical outcomes. Nonetheless, the ISL MAP simulations presented in this study provide insightful preliminary data for the investigation of ISL as a MAP candidate.

As mentioned, the dose loading implemented for the CAB and RPV MAP intradermal PBPK model [27] was applied

**Table 3** Predicted vs observed ISL pharmacokinetics following single-dose oral administration [17]

| Dose (mg) | Parameter | Observed | Predicted | Ratio | AAFE |
|---|---|---|---|---|---|
| 0.5 | AUC (ng·h/ml) | 11.23 | 15.25 ± 0.12 | 1.36 | 1.36 |
| | $C_{max}$ (ng/ml) | 5.97 | 3.41 ± 0. 51 | 0.57 | 1.75 |
| 1 | AUC (ng·h/ml) | 26.07 | 30.5 ± 0.26 | 1.17 | 1.17 |
| | $C_{max}$ (ng/ml) | 11.70 | 6.83 ± 1.19 | 0.58 | 1.71 |
| 2 | AUC (ng·h/ml) | 46.15 | 60.94 ± 0.51 | 1.32 | 1.32 |
| | $C_{max}$ (ng/ml) | 12.88 | 13.44 ± 2.34 | 1.04 | 1.04 |
| 10 | AUC (ng·h/ml) | 323.35 | 305.03 ± 2.63 | 0.94 | 1.06 |
| | $C_{max}$ (ng/ml) | 69.08 | 69.03 ± 11.86 | 1.00 | 1.00 |
| 30 | AUC (ng·h/ml) | 946.52 | 913.96 ± 7.79 | 0.97 | 1.04 |
| | $C_{max}$ (ng/ml) | 199.30 | 201.59 ± 36.45 | 1.01 | 1.01 |

Observed data [17] are presented as the mean of 6 PLWH. Predicted data are presented as the mean ± standard deviation from 100 simulated healthy patients, male and female, aged 18–60 years. AAFE was calculated as described in Eq. 4

*AUC* area under the curve, $C_{max}$ maximum plasma concentration, *AAFE* absolute average fold error

in this study due to the lack of available data for ISL MAPs. The dose loading per $cm^2$ of MAP has a direct impact on therapeutic area and overall MAP size, with higher amounts of drug per $cm^2$ of MAP resulting in smaller sizes. If the currently simulated 4.09 mg/$cm^2$ dose loading is unattainable for ISL MAPs, the maximum administration timeframe of 12 months could be reduced significantly. Conversely, if a dose loading greater than 4.09 mg/$cm^2$ can be achieved, the maximum administration could increase beyond 12 months. MAP size is an important factor from both implementation and patient acceptability perspectives. Although larger MAPs can contain greater amounts of drug and benefit from extended durations of protection, they could present challenges when applying them to different body sites, reducing discreetness and ease of use [47]. In this study, although differing MAP therapeutic areas could be calculated based on alternative dose loadings, the pharmacokinetics for each dose simulated herein would not necessarily be reflective of those resulting from other dose loading scenarios. This is a result of two factors. Firstly, dose loading is not only affected by a drug's physicochemical properties but also by the MAP design, such as microneedle shape and density [13, 14]. The MAP intradermal PBPK model contains mathematical descriptions of the specific MAP design to enable accurate simulation of drug movement throughout the skin layers to the systemic circulation. Therefore, the current model structure may not be able to account for alternative dose loadings that are the result of different MAP designs, reducing simulation accuracy and overall model reliability. Secondly, the current MAP intradermal PBPK model contains unknown parameters, of which CAB and RPV *in vivo* data from a specific MAP design with a dose loading of 4.09 mg/$cm^2$ were used for parameter estimation. Additional model verification with different MAP designs would be required to verify that

**Table 4** Predicted vs observed ISL-TP pharmacokinetics following single-dose oral administration of ISL [17]

| Dose (mg) | Parameter | Observed | Predicted | Ratio | AAFE |
|---|---|---|---|---|---|
| 0.5 | AUC (pmol·h/$10^6$ PBMCs) | 35.3 | 31.72 ± 0.46 | 0.90 | 1.11 |
| | $C_{max}$ (pmol/$10^6$ PBMCs) | 0.3 | 0.15 ± 0.008 | 0.50 | 2.00 |
| | $C_{168}$ (pmol/$10^6$ PBMCs) | 0.1 | 0.076 ± 0.001 | 0.76 | 1.32 |
| 1 | AUC (pmol·h/$10^6$ PBMCs) | 60 | 63.43 ± 0.95 | 1.06 | 1.06 |
| | $C_{max}$ (pmol/$10^6$ PBMCs) | 0.4 | 0.30 ± 0.017 | 0.75 | 1.33 |
| | $C_{168}$ (pmol/$10^6$ PBMCs) | 0.2 | 0.152 ± 0.002 | 0.76 | 1.32 |
| 2 | AUC (pmol·h/$10^6$ PBMCs) | 76.2 | 126.64 ± 1.91 | 1.66 | 1.66 |
| | $C_{max}$ (pmol/$10^6$ PBMCs) | 0.5 | 0.59 ± 0.034 | 1.18 | 1.18 |
| | $C_{168}$ (pmol/$10^6$ PBMCs) | 0.2 | 0.3 ± 0.004 | 1.25 | 1.25 |
| 10 | AUC (pmol·h/$10^6$ PBMCs) | 445 | 634.52 ± 9.84 | 1.43 | 1.43 |
| | $C_{max}$ (pmol/$10^6$ PBMCs) | 2.8 | 2.99 ± 0.17 | 1.07 | 1.07 |
| | $C_{168}$ (pmol/$10^6$ PBMCs) | 1 | 1.52 ± 0.022 | 1.52 | 1.52 |
| 30 | AUC (pmol·h/$10^6$ PBMCs) | 1380 | 1899.25 ± 28.95 | 1.38 | 1.38 |
| | $C_{max}$ (pmol/$10^6$ PBMCs) | 8.9 | 8.89 ± 0.51 | 1.00 | 1.00 |
| | $C_{168}$ (pmol/$10^6$ PBMCs) | 4.8 | 4.54 ± 0.065 | 0.95 | 1.06 |

Observed data [17] are presented as the mean of 6 PLWH. Predicted data are presented as the mean ± standard deviation from 100 simulated healthy patients, male and female, aged 18–60 years. AAFE was calculated as described in Eq. 4

*AUC* area under the curve, $C_{max}$ maximum plasma concentration, $C_{168}$ concentration at 168 h post-dose, *AAFE* absolute average fold error, *PBMCs* peripheral blood mononuclear cells

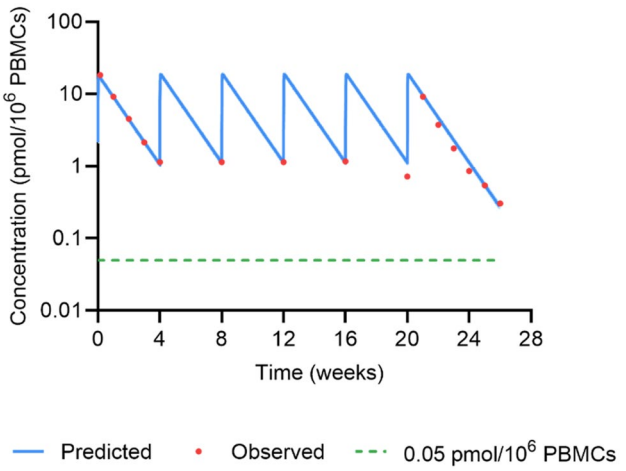


**Fig. 4** Observed vs predicted concentration–time profile of ISL-TP after once-monthly oral administration of 60 mg ISL. The *red circles* represent the mean of the observed clinical data (pmol/$10^6$ PBMCs) of ~ 100 HIV negative people [22]. The *blue line* represents the mean (pmol/$10^6$ PBMCs) of the predicted data. The *green dashed line* represents the minimum target concentration of 0.05 pmol/$10^6$ PBMCs [22]

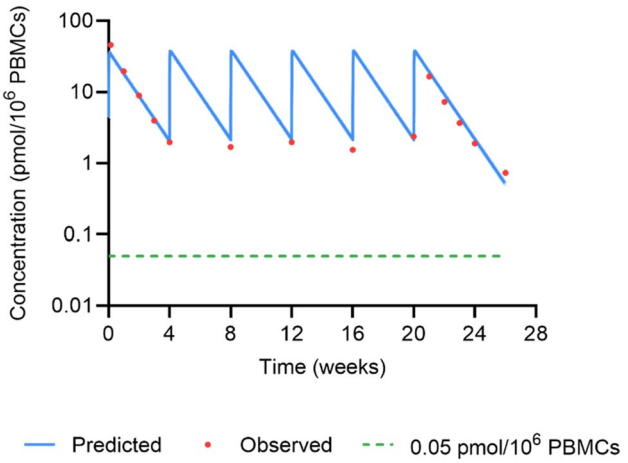


**Fig. 5** Observed vs predicted concentration–time profile of ISL-TP after once-monthly oral administration of 120 mg ISL. The *red circles* represent the mean of the observed clinical data (pmol/$10^6$ PBMCs) of ~ 100 HIV negative people [22]. The *blue line* represents the mean (pmol/$10^6$ PBMCs) of the predicted data. The *green dashed line* represents the minimum target concentration of 0.05 pmol/$10^6$ PBMCs [22]

these estimated parameters are applicable across all MAP intradermal PBPK models.

Whilst ISL MAPs show potential for long-acting administration, their clinical application must be taken into consideration. ISL is currently being assessed for both the prevention and treatment of HIV [17–22, 24]. In the case of pre-exposure prophylaxis (PrEP), ISL is being assessed alone; however, for treatment, ISL is being assessed as a three-drug regimen alongside doravirine (DOR) and lamivudine (3TC) [17]. For HIV treatment via MAP delivery, pairing ISL with another highly potent ARV such as lenacapavir would also be advantageous. Future research initiatives could apply the PBPK model used in this study to assess potential candidates together with ISL as two- or three-drug regimens for the treatment of HIV via MAP delivery. Additionally, as predicted by the PBPK model, the time taken to achieve the minimum target concentration after administration increased with decreasing nanoparticle release rates, bioavailability and dose. For successful prevention and treatment of HIV, concentrations within the therapeutic window must be achieved as quickly as possible [48]. It may therefore be necessary to consider an oral lead in of ISL for certain MAP designs to sustain appropriate concentrations over a shorter period of time. Furthermore, consideration must be made of the pharmacokinetic tail of ISL MAPs, with appropriate measures being made during clinical management. Specifically, as with any pharmacokinetic tail in long-acting ARV technologies, concerns surround the potential for the emergence of resistant HIV strains after long-acting treatment cessation [49, 50]. That being said, in December 2021, Merck published a news release stating that the FDA had placed clinical holds and partial clinical holds on several ISL clinical trials due to reported decreases in CD4+ T cells and total lymphocytes amongst some participants in the studies [51]. Whilst no further updates on the clinical holds have currently been published, the utility of this study remains, as it provides preliminary data and guidance on the design and application of ISL MAPs for the treatment and prevention of HIV.

## 5 Conclusion

A mathematical description of the conversion of ISL to ISL-TP was successfully verified. The PBPK model predicted the pharmacokinetics of ISL and ISL-TP up to 12 months after MAP administration, highlighting key characteristics such as dose and nanoparticle release rate required to sustain concentrations above the minimum target concentration with a favourable MAP therapeutic area. Based on the simulated data, ISL MAP doses of 80 mg were found to be suitable for 12-month administration, whilst doses as low as 15 mg were suitable for 6-month administration. This in silico study provides rationale for further investigation of ISL as a candidate for MAP administration if holds on ISL clinical trials employed by the FDA are lifted.

**Table 5** Predicted $C_{min}$ pharmacokinetics of 15 mg ISL MAPs 3, 6 and 12 months after administration

| Bioavailability (%) | Dose (mg) | Release rate ($h^{-1}$) | ISL-TP $C_{min}$ (pmol/$10^6$ PBMCs) | | | Time to reach target concentration (h) |
|---|---|---|---|---|---|---|
| | | | Month 3 | Month 6 | Month 12 | |
| 100 | 15 | 0.005 | 0.0047 ± 0.001 | 0 | 0 | 5 |
| | | 0.0025 | 0.0416 ± 0.0025 | 0.0003 ± 0 | 0 | 8 |
| | | 0.0005 | 0.2275 ± 0.0014[a] | 0.0831 ± 0.0006[a] | 0.0111 ± 0.0001 | 26 |
| 75 | 11.25 | 0.005 | 0.0034 ± 0.0007 | 0 | 0 | 6 |
| | | 0.0025 | 0.0311 ± 0.0019 | 0.0002 ± 0 | 0 | 9 |
| | | 0.0005 | 0.1709 ± 0.0012[a] | 0.0624 ± 0.0004[a] | 0.0083 ± 0.0001 | 35 |
| 50 | 7.5 | 0.005 | 0.0022 ± 0.0005 | 0 | 0 | 8 |
| | | 0.0025 | 0.0208 ± 0.0013 | 0.0001 ± 0 | 0 | 13 |
| | | 0.0005 | 0.1144 ± 0.0008[a] | 0.0418 ± 0.0003 | 0.0056 ± 0 | 53 |
| 25 | 3.75 | 0.005 | 0.0011 ± 0.0003 | 0 | 0 | 14 |
| | | 0.0025 | 0.0104 ± 0.0006 | 0.0001 ± 0 | 0 | 23 |
| | | 0.0005 | 0.0574 ± 0.0004[a] | 0.0211 ± 0.0002 | 0.0028 ± 0 | 119 |

MAP was simulated with a dose loading of 4.09 mg/$cm^2$ and a MAP therapeutic area of 3.67 $cm^2$. Predicted ISL-TP $C_{min}$ data are presented as the mean ± standard deviation from 100 simulated healthy patients, male and female, aged 18–60 years 3, 6 and 12 months after MAP administration. Bioavailability is defined as the percent of drug reaching the systemic circulation from MAP administration. Doses correspond to the outlined bioavailability percentages simulated in the PBPK model. A minimum target ISL-TP concentration of 0.05 pmol/$10^6$ PBMCs was applied

*$C_{min}$* minimum plasma concentration, *PBMCs* peripheral blood mononuclear cells, *ISL-TP* islatravir triphosphate

[a]$C_{min}$ concentrations above the minimum target ISL-TP concentration

**Table 6** Predicted $C_{min}$ pharmacokinetics of 30 mg ISL MAPs 3, 6 and 12 months after administration

| Bioavailability (%) | Dose (mg) | Release rate ($h^{-1}$) | ISL-TP $C_{min}$ (pmol/$10^6$ PBMCs) | | | Time to reach target concentration (h) |
|---|---|---|---|---|---|---|
| | | | Month 3 | Month 6 | Month 12 | |
| 100 | 30 | 0.005 | 0.0135 ± 0.0029 | 0 | 0 | 3 |
| | | 0.0025 | 0.1243 ± 0.0075[a] | 0.0008 ± 0.0001 | 0 | 4 |
| | | 0.0005 | 0.4545 ± 0.0032[a] | 0.1659 ± 0.0012[a] | 0.0221 ± 0.0002 | 14 |
| 75 | 22.5 | 0.005 | 0.0069 ± 0.0016 | 0 | 0 | 4 |
| | | 0.0025 | 0.0628 ± 0.0036[a] | 0.0004 ± 0 | 0 | 6 |
| | | 0.0005 | 0.3414 ± 0.0024[a] | 0.1247 ± 0.0009[a] | 0.0166 ± 0.0001 | 18 |
| 50 | 15 | 0.005 | 0.0047 ± 0.001 | 0 | 0 | 5 |
| | | 0.0025 | 0.0416 ± 0.0025 | 0.0003 ± 0 | 0 | 8 |
| | | 0.0005 | 0.2275 ± 0.0014[a] | 0.0831 ± 0.0006[a] | 0.0111 ± 0.0001 | 26 |
| 25 | 7.5 | 0.005 | 0.0022 ± 0.0005 | 0 | 0 | 8 |
| | | 0.0025 | 0.0208 ± 0.0013 | 0.0001 ± 0 | 0 | 13 |
| | | 0.0005 | 0.1144 ± 0.0008[a] | 0.0418 ± 0.0003 | 0.0056 ± 0 | 53 |

MAP was simulated with a dose loading of 4.09 mg/$cm^2$ and a MAP therapeutic area of 7.34 $cm^2$. Predicted ISL-TP $C_{min}$ data are presented as the mean ± standard deviation from 100 simulated healthy patients, male and female, aged 18–60 years 3, 6 and 12 months after MAP administration. Bioavailability is defined as the percent of drug reaching the systemic circulation from MAP administration. Doses correspond to the outlined bioavailability percentages simulated in the PBPK model. A minimum target ISL-TP concentration of 0.05 pmol/$10^6$ PBMCs was applied

*$C_{min}$* minimum plasma concentration, *PBMCs* peripheral blood mononuclear cells, *ISL-TP* islatravir triphosphate

[a]$C_{min}$ concentrations above the minimum target ISL-TP concentration

**Table 7** Predicted $C_{min}$ pharmacokinetics of 60 mg ISL MAPs 3, 6 and 12 months after administration

| Bioavailability (%) | Dose (mg) | Release rate ($h^{-1}$) | ISL-TP $C_{min}$ (pmol/$10^6$ PBMCs) | | | Time to reach target concentration (h) |
|---|---|---|---|---|---|---|
| | | | Month 3 | Month 6 | Month 12 | |
| 100 | 60 | 0.005 | 0.0187 ± 0.0042 | 0 | 0 | 3 |
| | | 0.0025 | 0.1684 ± 0.0107[a] | 0.0011 ± 0.0001 | 0 | 4 |
| | | 0.0005 | 0.9098 ± 0.0063[a] | 0.3321 ± 0.0024[a] | 0.0442 ± 0.0003 | 9 |
| 75 | 45 | 0.005 | 0.0134 ± 0.0031 | 0 | 0 | 3 |
| | | 0.0025 | 0.1256 ± 0.0073[a] | 0.0008 ± 0.0001 | 0 | 4 |
| | | 0.0005 | 0.6815 ± 0.0046[a] | 0.2488 ± 0.0017[a] | 0.0332 ± 0.0002 | 10 |
| 50 | 30 | 0.005 | 0.0135 ± 0.0029 | 0 | 0 | 3 |
| | | 0.0025 | 0.1243 ± 0.0075[a] | 0.0008 ± 0.0001 | 0 | 4 |
| | | 0.0005 | 0.4545 ± 0.0032[a] | 0.1659 ± 0.0012[a] | 0.0221 ± 0.0002 | 14 |
| 25 | 15 | 0.005 | 0.0047 ± 0.001 | 0 | 0 | 5 |
| | | 0.0025 | 0.0416 ± 0.0025[a] | 0.0003 ± 0 | 0 | 8 |
| | | 0.0005 | 0.2275 ± 0.0014[a] | 0.0831 ± 0.0006[a] | 0.0111 ± 0.0001 | 26 |

MAP was simulated with a dose loading of 4.09 mg/$cm^2$ and a MAP therapeutic area of 14.68 $cm^2$. Predicted ISL-TP $C_{min}$ data are presented as the mean ± standard deviation from 100 simulated healthy patients, male and female, aged 18–60 years 3, 6 and 12 months after MAP administration. Bioavailability is defined as the percent of drug reaching the systemic circulation from MAP administration. Doses correspond to the outlined bioavailability percentages simulated in the PBPK model. A minimum target ISL-TP concentration of 0.05 pmol/$10^6$ PBMCs was applied

*$C_{min}$* minimum plasma concentration, *PBMCs* peripheral blood mononuclear cells, *ISL-TP* islatravir triphosphate

[a]$C_{min}$ concentrations above the minimum target ISL-TP concentration

**Table 8** Predicted $C_{min}$ pharmacokinetics of 80 mg ISL MAPs 3, 6 and 12 months after administration

| Bioavailability (%) | Dose (mg) | Release rate ($h^{-1}$) | ISL-TP $C_{min}$ (pmol/$10^6$ PBMCs) | | | Time to reach target concentration (h) |
|---|---|---|---|---|---|---|
| | | | Month 3 | Month 6 | Month 12 | |
| 100 | 80 | 0.005 | 0.0232 ± 0.0055 | 0 | 0 | 2 |
| | | 0.0025 | 0.222 ± 0.0156[a] | 0.0015 ± 0.0001 | 0 | 3 |
| | | 0.0005 | 1.2128 ± 0.0081[a] | 0.4428 ± 0.0031[a] | 0.0590 ± 0.0004[a] | 7 |
| 75 | 60 | 0.005 | 0.0187 ± 0.0042 | 0 | 0 | 3 |
| | | 0.0025 | 0.1684 ± 0.0107[a] | 0.0011 ± 0.0001 | 0 | 4 |
| | | 0.0005 | 0.9098 ± 0.0063[a] | 0.3321 ± 0.0024[a] | 0.0442 ± 0.0003 | 9 |
| 50 | 40 | 0.005 | 0.0126 ± 0.0032 | 0 | 0 | 3 |
| | | 0.0025 | 0.1109 ± 0.0066[a] | 0.0007 ± 0.0001 | 0 | 4 |
| | | 0.0005 | 0.6066 ± 0.0046[a] | 0.2215 ± 0.0017[a] | 0.0295 ± 0.0002 | 12 |
| 25 | 20 | 0.005 | 0.0062 ± 0.0013 | 0 | 0 | 5 |
| | | 0.0025 | 0.0559 ± 0.0034[a] | 0.0004 ± 0 | 0 | 7 |
| | | 0.0005 | 0.3038 ± 0.0021[a] | 0.1109 ± 0.0008[a] | 0.0148 ± 0.0001 | 21 |

MAP was simulated with a dose loading of 4.09 mg/$cm^2$ and a MAP therapeutic area of 19.57 $cm^2$. Predicted ISL-TP $C_{min}$ data are presented as the mean ± standard deviation from 100 simulated healthy patients, male and female, aged 18–60 years 3, 6 and 12 months after MAP administration. Bioavailability is defined as the percent of drug reaching the systemic circulation from MAP administration. Doses correspond to the outlined bioavailability percentages simulated in the PBPK model. A minimum target ISL-TP concentration of 0.05 pmol/$10^6$ PBMCs was applied

*$C_{min}$* minimum plasma concentration, *PBMCs* peripheral blood mononuclear cells, *ISL-TP* islatravir triphosphate

[a]$C_{min}$ concentrations above the minimum target ISL-TP concentration

**Supplementary Information** The online version contains supplementary material available at https://doi.org/10.1007/s13318-022-00793-6.

## Declarations

**Funding** This study was funded with UK aid from the UK government through the Foreign Commonwealth and Development Office.

**Conflict of interest** Author Marco Siccardi has received research grant funding from Janssen and ViiV and is currently an employee of Labcorp. Authors Hannah Kinvig, Nicolas Cottura, Andrew Lloyd, Collrane Frivold, Jessica Mistilis and Courtney Jarrahian declare that they have no conflict of interest.

**Ethics approval** Not applicable.

**Consent to participate** Not applicable.

**Consent for publication** Not applicable.

**Availability of data and material** All data generated during this study are included in this published article and its supplementary information files.

**Code availability** Not applicable.

**Authors' contributions** All authors contributed to the study conception and design. Model development, simulations and analysis were carried out by Hannah Kinvig, Nicolas Cottura, Andrew Lloyd and Marco Siccardi. The first draft of the manuscript was written by Hannah Kinvig and all authors commented on previous versions of the manuscript. All authors read and approved the final manuscript.



## References

1. UNAIDS. Global HIV and AIDS statistics—2020 fact sheet. 2020. https://www.unaids.org/en/resources/fact-sheet. Accessed 17 Feb 2021.
2. CDC. Pre-exposure prophylaxis (PrEP) and post-exposure prophylaxis (PEP). 2020. https://www.cdc.gov/hiv/clinicians/prevention/prep-and-pep.html#:~:text=Syndicate-,Pre%2DExposure%20Prophylaxis%20(PrEP)%20and,Post%2DExposure%20Prophylaxis%20(PEP)&text=PrEP%20is%20a%20prevention%20method,contact%20or%20injection%20drug%20use. Accessed 18 Feb 2021.
3. WHO. Update of recommendations on first- and second-line antiretroviral regimens. Geneva: World Health Organisation; 2019.
4. Maartens G, Celum C, Lewin SR. HIV infection: epidemiology, pathogenesis, treatment, and prevention. Lancet. 2014;384(9939):258–71. https://doi.org/10.1016/S0140-6736(14)60164-1.
5. Kirchhoff F. HIV life cycle: overview. In: Hope TJ, Stevenson M, Richman D, editors. Encyclopedia of AIDS. New York: Springer; 2013. p. 1–9.
6. NIH. FDA-approved HIV medicines. 2021. https://hivinfo.nih.gov/understanding-hiv/fact-sheets/fda-approved-hiv-medicines. Accessed 18 Feb 2021.
7. Menéndez-Arias L, Martín-Alonso S, Frutos-Beltrán E. An update on antiretroviral therapy. In: Liu X, Zhan P, Menéndez-Arias L, Poongavanam V, editors. Antiviral drug discovery and development. Singapore: Springer Singapore; 2021.
8. Cobb DA, Smith NA, Edagwa BJ, McMillan JM. Long-acting approaches for delivery of antiretroviral drugs for prevention and treatment of HIV: a review of recent research. Expert Opin Drug Deliv. 2020;17(9):1227–38. https://doi.org/10.1080/17425247.2020.1783233.
9. Scarsi KK, Swindells S. The promise of improved adherence with long-acting antiretroviral therapy: what are the data? J Int Assoc Provid AIDS Care. 2021;20:23259582211009012. https://doi.org/10.1177/23259582211009011.
10. FDA. FDA approves first extended-release, injectable drug regimen for adults living with HIV. 2021. https://www.fda.gov/news-events/press-announcements/fda-approves-first-extended-release-injectable-drug-regimen-adults-living-hiv. Accessed 19 Feb 2021.
11. Overton ET, Richmond G, Rizzardini G, Jaeger H, Orrell C, Nagimova F, et al. Long-acting cabotegravir and rilpivirine dosed every 2 months in adults with HIV-1 infection (ATLAS-2M), 48-week results: a randomised, multicentre, open-label, phase 3b, non-inferiority study. Lancet. 2021;396(10267):1994–2005. https://doi.org/10.1016/S0140-6736(20)32666-0.
12. Halder J, Gupta S, Kumari R, Gupta GD, Rai VK. Microneedle array: applications, recent advances, and clinical pertinence in transdermal drug delivery. J Pharm Innov. 2020. https://doi.org/10.1007/s12247-020-09460-2.
13. Paredes AJ, Ramoller IK, McKenna PE, Abbate MTA, Volpe-Zanutto F, Vora LK, et al. Microarray patches: Breaking down the barriers to contraceptive care and HIV prevention for women across the globe. Adv Drug Deliv Rev. 2021;173:331–48. https://doi.org/10.1016/j.addr.2021.04.002.
14. Vora LK, Moffatt K, Tekko IA, Paredes AJ, Volpe-Zanutto F, Mishra D, et al. Microneedle array systems for long-acting drug delivery. Eur J Pharm Biopharm. 2021;159:44–76. https://doi.org/10.1016/j.ejpb.2020.12.006.
15. Dugam S, Tade R, Dhole R, Nangare S. Emerging era of microneedle array for pharmaceutical and biomedical applications: recent advances and toxicological perspectives. Future J Pharm Sci. 2021;7(1):19. https://doi.org/10.1186/s43094-020-00176-1.
16. Jung JH, Jin SG. Microneedle for transdermal drug delivery: current trends and fabrication. J Pharm Investig. 2021. https://doi.org/10.1007/s40005-021-00512-4.
17. Schurmann D, Rudd DJ, Zhang S, De Lepeleire I, Robberechts M, Friedman E, et al. Safety, pharmacokinetics, and antiretroviral activity of islatravir (ISL, MK-8591), a novel nucleoside reverse transcriptase translocation inhibitor, following single-dose administration to treatment-naive adults infected with HIV-1: an open-label, phase 1b, consecutive-panel trial. Lancet HIV. 2020;7(3):e164–72. https://doi.org/10.1016/S2352-3018(19)30372-8.
18. Molina JM, Yazdanpanah Y, Afani Saud A, Bettacchi C, Chahin Anania C, DeJesus E, et al. Islatravir in combination with doravirine for treatment-naive adults with HIV-1 infection receiving initial treatment with islatravir, doravirine, and lamivudine: a phase 2b, randomised, double-blind, dose-ranging trial. Lancet

HIV. 2021;8(6):e324–33. https://doi.org/10.1016/S2352-3018(21)00021-7.
19. Matthews RP, Patel M, Barrett SE, Haspeslagh L, Reynders T, Zhang S, et al. Safety and pharmacokinetics of islatravir subdermal implant for HIV-1 pre-exposure prophylaxis: a randomized, placebo-controlled phase 1 trial. Nat Med. 2021;27(10):1712–7. https://doi.org/10.1038/s41591-021-01479-3.
20. Markowitz M, Sarafianos SG. 4′-Ethynyl-2-fluoro-2′-deoxyadenosine, MK-8591: a novel HIV-1 reverse transcriptase translocation inhibitor. Curr Opin HIV AIDS. 2018;13(4):294–9. https://doi.org/10.1097/COH.0000000000000467.
21. Barrett SE, Teller RS, Forster SP, Li L, Mackey MA, Skomski D, et al. Extended-duration MK-8591-eluting implant as a candidate for HIV treatment and prevention. Antimicrob Agents Chemother. 2018. https://doi.org/10.1128/AAC.01058-18.
22. Hillier S, Badal-Faesen S, Hendrix CW, Riddler SA, Rasmussen S, Schwartz H, Nair G, Lombaard JH, Caraco Y, Peer A, Patel M, Evans B, Homony B, Teal V, Hwang P, Robertson M, Plank R. Trial design, enrollment status, demographics, and pharmacokinetics (PK) data from a blinded interim analysis from a phase 2a trial of Islatravir once monthly (QM) for HIV pre-exposure prophylaxis (PrEP). HIVR4P 2021 (virtual event); 2021 Jan 27–28 & Feb 3–4.
23. Michailidis E, Huber AD, Ryan EM, Ong YT, Leslie MD, Matzek KB, et al. 4'-Ethynyl-2-fluoro-2′-deoxyadenosine (EFdA) inhibits HIV-1 reverse transcriptase with multiple mechanisms. J Biol Chem. 2014;289(35):24533–48. https://doi.org/10.1074/jbc.M114.562694.
24. Rudd DJ, Cao Y, Vaddady P, Grobler JA, Asante-Appiah E, Diamond T, Klopfer S, Grandhi A, Sklar P, Hwang C, Vargo R. Modeling-supported islatravir dose selection for phase III. In: Conference on Retroviruses and Opportunistic Infections; 2020 March 8–11; Boston.
25. Bleasby K, Houle R, Hafey M, Lin M, Guo J, Lu B, et al. Islatravir is not expected to be a victim or perpetrator of drug–drug interactions via major drug-metabolizing enzymes or transporters. Viruses. 2021;13(8):1566. https://doi.org/10.3390/v13081566.
26. Peters SA. Physiologically-based pharmacokinetic (PBPK) modeling and simulations: principles, methods, and applications in the pharmaceutical industry. 1st ed. Hoboken: Wiley; 2012.
27. Rajoli RKR, Flexner C, Chiong J, Owen A, Donnelly RF, Larraneta E, et al. Modelling the intradermal delivery of microneedle array patches for long-acting antiretrovirals using PBPK. Eur J Pharm Biopharm. 2019;144:101–9. https://doi.org/10.1016/j.ejpb.2019.09.011.
28. Gajewska M, Worth A, Urani C, Briesen H, Schramm KW. Application of physiologically-based toxicokinetic modelling in oral-to-dermal extrapolation of threshold doses of cosmetic ingredients. Toxicol Lett. 2014;227(3):189–202. https://doi.org/10.1016/j.toxlet.2014.03.013.
29. Fryar CD, Gu Q, Ogden CL, Flegal KM. Anthropometric reference data for children and adults: United States, 2011–2014. National Center for Health Statistics. Vital Health Stat 3(39). 2016.
30. Bosgra S, van Eijkeren J, Bos P, Zeilmaker M, Slob W. An improved model to predict physiologically based model parameters and their inter-individual variability from anthropometry. Crit Rev Toxicol. 2012;42(9):751–67. https://doi.org/10.3109/10408444.2012.709225.
31. Shuter B, Aslani A. Body surface area: Du Bois and Du Bois revisited. Eur J Appl Physiol. 2000;82(3):250–4. https://doi.org/10.1007/s004210050679.
32. Brown RP, Delp MD, Lindstedt SL, Rhomberg LR, Beliles RP. Physiological parameter values for physiologically based pharmacokinetic models. Toxicol Ind Health. 1997;13(4):407–84. https://doi.org/10.1177/074823379701300401.
33. Rajoli RKR. Investigation of long-acting antiretroviral nanoformulation pharmacokinetics using experimental and computational methods. PhD thesis. Liverpool: University of Liverpool; 2017.
34. Peters SA. Evaluation of a generic physiologically based pharmacokinetic model for lineshape analysis. Clin Pharmacokinet. 2008;47(4):261–75. https://doi.org/10.2165/00003088-200847040-00004.
35. Yu LX, Amidon GL. A compartmental absorption and transit model for estimating oral drug absorption. Int J Pharm. 1999;186(2):119–25. https://doi.org/10.1016/s0378-5173(99)00147-7.
36. Poulin P, Theil FP. Prediction of pharmacokinetics prior to in vivo studies. 1. Mechanism-based prediction of volume of distribution. J Pharm Sci. 2002;91(1):129–56. https://doi.org/10.1002/jps.10005.
37. Kinvig H. Integrated experimental and computational approaches for the prediction of drug–drug interactions. Liverpool: University of Liverpool; 2021.
38. Paixao P, Gouveia LF, Morais JA. Prediction of drug distribution within blood. Eur J Pharm Sci. 2009;36(4–5):544–54. https://doi.org/10.1016/j.ejps.2008.12.011.
39. National Center for Biotechnology Information. PubChem. 4′-Ethynyl-2-Fluoro-2′-Deoxyadenosine, CID=6483431. https://pubchem.ncbi.nlm.nih.gov/compound/6483431]. Accessed 30 Sept 2021.
40. ChemSpider. 9-(2-Deoxy-4-ethynyl-D-erythro-pentofuranosyl)-2-fluoro-9H-purin-6-amine. http://www.chemspider.com/ChemicalStructure.57577941.html?rid=52efdc8b-3abe-49a6-8c43-7c861e5e412d&page_num=0]. Accessed 30 Sept 2021.
41. Zhang W, Parniak MA, Sarafianos SG, Empey PE, Rohan LC. In vitro transport characteristics of EFdA, a novel nucleoside reverse transcriptase inhibitor using Caco-2 and MDCKII cell monolayers. Eur J Pharmacol. 2014;732:86–95. https://doi.org/10.1016/j.ejphar.2014.03.022.
42. DrugBank. Islatravir. 2020. https://go.drugbank.com/drugs/DB15653. Accessed 30 Sept 2021.
43. Stoddart CA, Galkina SA, Joshi P, Kosikova G, Moreno ME, Rivera JM, et al. Oral administration of the nucleoside EFdA (4′-ethynyl-2-fluoro-2′-deoxyadenosine) provides rapid suppression of HIV viremia in humanized mice and favorable pharmacokinetic properties in mice and the rhesus macaque. Antimicrob Agents Chemother. 2015;59(7):4190–8. https://doi.org/10.1128/AAC.05036-14.
44. Njai HF, Gombe B, Khamis T, Birungi J, Ruzagira E, Admassu D, et al. Setting up a standardized peripheral blood mononuclear cells processing laboratory to support multi-center HIV/AIDS vaccine and intervention trials. Lab Med. 2011;42(12):711–8. https://doi.org/10.1309/LM84WWEUSKT4ABXO (%**J Laboratory Medicine**).
45. Shebley M, Sandhu P, Emami Riedmaier A, Jamei M, Narayanan R, Patel A, et al. Physiologically based pharmacokinetic model qualification and reporting procedures for regulatory submissions: a consortium perspective. Clin Pharmacol Ther. 2018;104(1):88–110. https://doi.org/10.1002/cpt.1013.
46. Riley RJ, McGinnity DF, Austin RP. A unified model for predicting human hepatic, metabolic clearance from in vitro intrinsic clearance data in hepatocytes and microsomes. Drug Metab Dispos. 2005;33(9):1304–11. https://doi.org/10.1124/dmd.105.004259.
47. Brook MK, Ismail A, Magni S, Fellows T, Katahoire AR, Ayebare F, et al. User assessment of a microarray patch for HIV PrEP and as a multipurpose prevention technology for HIV and pregnancy prevention: perspectives from Uganda and South Africa. J Int AIDS Soc. 2021;24:10.
48. Saag MS. HIV 101: fundamentals of antiretroviral therapy. Top Antivir Med. 2019;27(3):123–7.

49. Landovitz RJ, Kofron R, McCauley M. The promise and pitfalls of long-acting injectable agents for HIV prevention. Curr Opin HIV AIDS. 2016;11(1):122–8. https://doi.org/10.1097/COH.0000000000000219.
50. Hodge D, Back DJ, Gibbons S, Khoo SH, Marzolini C. Pharmacokinetics and drug–drug interactions of long-acting intramuscular cabotegravir and rilpivirine. Clin Pharmacokinet. 2021;60(7):835–53. https://doi.org/10.1007/s40262-021-01005-1.
51. Merck. Merck announces clinical holds on studies evaluating islatravir for the treatment and prevention of HIV-1 infection. Press release. 2021. https://www.merck.com/news/merck-announces-clinical-holds-on-studies-evaluating-islatravir-for-the-treatment-and-prevention-of-hiv-1-infection/. Accessed 2021 December 20.

## Authors and Affiliations

**Hannah Kinvig[1] · Nicolas Cottura[1] · Andrew Lloyd[1] · Collrane Frivold[2] · Jessica Mistilis[2] · Courtney Jarrahian[2] · Marco Siccardi[1]**

✉ Hannah Kinvig
hmkinvig@liverpool.ac.uk

[1] Department of Pharmacology and Therapeutics, Institute of Systems, Molecular and Integrative Biology, University of Liverpool, 70 Pembroke Place, Liverpool L69 3GF, UK

[2] Medical Devices and Health Technologies Global Program, PATH, Seattle, USA